Received: 4 July 2023 | Revised: 23 October 2023 | Accepted: 11 December 2023

DOI: 10.1002/cyto.a.24822

ORIGINAL ARTICLE

MIFlowCyt

ISAC INTERNATIONAL SOCIETY FOR ADVANCEMENT OF CYTOMETRY

CYTOMETRY Journal of Quantitative Cell Science PART A

Fluorescent characterization of differentiated myotubes using flow cytometry

Andy Nolan[1,2] | Robert A. Heaton[2] | Petra Adamova[3] | Paige Cole[1] | Nadia Turton[3] | Scott H. Gillham[1] | Daniel J. Owens[1] | Darren W. Sexton[3]

[1]Research Institute for Sport and Exercise Sciences, Liverpool John Moores University, Liverpool, UK

[2]Institute of Life Course and Medical Sciences, University of Liverpool, Liverpool, UK

[3]School of Pharmacy and Biomolecular Sciences, Liverpool John Moores University, Liverpool, UK

Correspondence
Darren W. Sexton, School of Pharmacy and Biomolecular Sciences, Liverpool John Moores University, Liverpool, UK.
Email: d.w.sexton@ljmu.ac.uk

Funding information
Rank Prize Fund New Lecturers Award; Liverpool John Moores University

Abstract

Flow cytometry is routinely used in the assessment of skeletal muscle progenitor cell (myoblast) populations. However, a full gating strategy, inclusive of difficult to interpret forward and side scatter data, which documents cytometric analysis of differentiated myoblasts (myotubes) has not been reported. Beyond changes in size and shape, there are substantial metabolic and protein changes in myotubes allowing for their potential identification within heterogenous cell suspensions. To establish the utility of flow cytometry for determination of myoblasts and myotubes, C2C12 murine cell populations were assessed for cell morphology and metabolic reprogramming. Laser scatter, both forward (FSC; size) and side (SSC; granularity), measured cell morphology, while mitochondrial mass, reactive oxygen species (ROS) generation and DNA content were quantified using the fluorescent probes, MitoTracker green, CM-H_2DCFDA and Vybrant DyeCycle, respectively. Immunophenotyping for myosin heavy chain (MyHC) was utilized to confirm myotube differentiation. Cellular viability was determined using Annexin V/propidium iodide dual labelling. Fluorescent microscopy was employed to visualize fluorescence and morphology. Myotube and myoblast populations were resolvable through non-intuitive interpretation of laser scatter-based morphology assessment and mitochondrial mass and activity assessment. Myotubes appeared to have similar sizes to the myoblasts based on laser scatter but exhibited greater mitochondrial mass (159%, $p < 0.0001$), ROS production (303%, $p < 0.0001$), DNA content (18%, $p < 0.001$) and expression of MyHC (147%, $p < 0.001$) compared to myoblasts. Myotube sub-populations contained a larger viable cluster of cells which were unable to be fractionated from myoblast populations and a smaller population cluster which likely contains apoptotic bodies. Imaging of differentiated myoblasts that had transited through the flow cytometer revealed the presence of intact, 'rolled-up' myotubes, which would alter laser scatter properties

and potential transit through the laser beam. Our results indicate that myotubes can be analyzed successfully using flow cytometry. Increased mitochondrial mass, ROS and DNA content are key features that correlate with MyHC expression but due to myotubes 'rolling up' during flow cytometric analysis, laser scatter determination of size is not positively correlated; a phenomenon observed with some size determination particles and related to surface properties of said particles. We also note a greater heterogeneity of myotubes compared to myoblasts as evidenced by the 2 distinct sub-populations. We suggest that acoustic focussing may prove effective in identifying myotube sub populations compared to traditional hydrodynamic focussing.

KEYWORDS
C2C12, flow cytometry, myoblasts, myotubes

1 | INTRODUCTION

During embryonic development, several phases of cellular proliferation and differentiation lead to the fusing of mononucleated myoblasts to form multinucleated myofibers, in a process known as myogenesis [1]. This process is facilitated through the coordinated expression of transcription factors including *Pax3* and a number of myogenic regulatory factors (MRF's) [2]. The in vitro replication of this process can be achieved through the culture of skeletal myoblasts and induction of differentiation by reduction in serum growth factors, leading to the formation of myotubes [3]. These myotubes better represent the conformation and metabolic properties of skeletal muscle in vivo when compared to myoblasts and consequently, are routinely used as a model of analyzing skeletal muscle metabolism and signaling [4].

Despite the frequent use of myotubes as an in vitro model, cytometry-based analysis of muscle is typically utilized only in myoblasts. This is perhaps due to the relatively large size of myotubes, with cellular diameters ranging from ~5 to 25 μm [5], increasing the likelihood of instrumental blockage. Due to the perceived limitations of flow cytometry for the analysis of myoblast and myotube cultures, there are no reports of the morphological characteristics of myoblasts compared to myotubes by flow cytometry [6–9], nor application of the technology for fluorescence-based assessment of cell phenotype and function. Immunocytochemistry using the intracellularly expressed motor protein myosin heavy chain (MyHC) has often been utilized to quantify myoblast differentiation [10]. MyHC, which converts chemical energy derived from adenosine triphosphate (ATP) into mechanical force, is expressed almost entirely in differentiating myotubes, with very low expression present in myoblasts, thus, allowing for myoblast-independent muscle identification [11–17].

Intracellular immunophenotyping is, however, expensive and involves considerable processing, inclusive of fixation and permeabilization which renders cells non-viable. Ideally, researchers would like to both analyze cells and identify sub-populations for further analysis, and fractionate mixed populations into unique phenotypes such as myoblasts and myotubes, which can be sorted for downstream analyses such as single cell transcriptomics. Flow cytometry provides such an opportunity if appropriate probes can be used. Given that myotube cell populations will typically include undifferentiated myoblasts in the cell suspension, there is a possibility that the myoblast population within the sample may be analyzed independently of the myotubes based on their morphological characteristics, fluorescent probes for organelle mass and activity, and cell surface immunophenotyping. Myogenic differentiation is associated with extensive metabolic remodeling, with myotubes shown to possess higher quantities of mitochondrial proteins and enzymes [18]. This increase in protein content reflects an overall increase in mitochondrial mass and activity [19]. Furthermore, this increase in mitochondrial content and respiratory chain activity has been linked to greater production of reactive oxygen species (ROS), highlighting the potential utility of metabolic biomarkers for the identification of muscle subpopulations [20]. We proposed that metabolic assessment of a mixed population of myotubes and myoblasts, using simple, easy to use, metabolism-related fluorescent probes may accurately distinguish the phenotype of the cells.

Flow cytometry and immunocytochemistry were conducted to monitor the fluorescent changes in C2C12 myoblast/myotube metabolic phenotype and protein expression. We set out to demonstrate that myotubes can be fluorescently detected using flow cytometry as depicted by the expected increase in mitochondrial content, ROS production and DNA content. Moreover, myotubes also expressed increased MyHC expression compared to myoblasts suggesting muscle differentiation. We also demonstrated that myotubes form 2 distinct populations, with one larger viable population which shares morphological similarities with the myoblast group, and another smaller population which likely contains apoptotic bodies. Moreover, we found that the morphological characterization of myotubes was non-intuitive due to the 'rolling-up' of myotubes (a previously unexplained factor that may have dissuaded researchers from using flow cytometry) but nevertheless confirmed the presence of intact myotubes following cytometric analysis. We, therefore, provide a transparent rationale for the utilization and analysis of myotube sub-populations using flow cytometry.

TABLE 1 Fluorescent dye information.

Antibody/dye	Analyte	Concentration	λ_{ex}[a]	λ_{em}[b]
MitoTracker green	Mitochondrial mass	100 nM	488 nm	533/30 nm FL-1
CM-H_2DCFDA	Reactive oxygen species	1 mM	488 nm	533/30 nm FL-1
Vibrant DyeCycle Ruby stain	DNA content	5 μM	640 nm	675/25 FL-4
Annexin V	Phosphatidylserine exposure	5uL[c]	488 nm	533/30 nm FL-1
Propidium iodide	Membrane integrity	1 μg/mL	488 nm	670 LP FL-3
Alexa fluor 488	MyHC expression	2 mM	488 nm	533/30 nm FL-1

[a]Excitation Wavelength on BD Accuri C6.
[b]Emission wavelengths measured on BD Accuri C6.
[c]Manufacturer recommended volume but no concentration given.

2 | METHODS

2.1 | C2C12 population expansion and differentiation

A C2C12 myoblast population (ATCC; Rockville, USA) was expanded at 37°C/5% CO_2/humidified air using growth medium (GM) containing Dulbecco's modified eagles medium (DMEM) with added L-glutamine (2.5 mM) and glucose (4,500 $mg.L^{-1}$) (Sigma-Aldrich Company Ltd. Dorset, UK), 20% foetal bovine serum (FBS) (Life Technologies. California, USA) and 1% PenStrep solution (50 units penicillin/ 50 μg streptomycin) (Life Technologies. California, USA). Cells were cultured until they reached 80% confluency. For myotube experiments the cell medium was aspirated, cells were then washed × 2 with PBS (Sigma-Aldrich Company Ltd. Dorset, UK) and replaced with differentiation medium (DM) containing DMEM, 2% horse serum (Life Technologies. California, USA) and 1% PenStrep solution. Cells were differentiated for 7 days (37°C/5% CO_2/humidified air), with existing media replaced every 48 h.

2.2 | Flow cytometry

For each sample, 20,000 gated events were recorded using a BD-Accuri C6 Flow Cytometer (BD, New Jersey, USA) equipped with a blue (488 nm) and red laser (640 nm). Gated events included cells and excluded cellular debris. For all experiments, cells were trypsinised before centrifugation and resuspended in filtered PBS for analysis. Preliminary experiments were performed to establish the optimal core size, flow rate and seeding density which were used in subsequent experiments. All samples, thereafter, were run at 35 uL/min representing a core size of 16 mm, at a cell seeding density of 1×10^{-6}/mL. Table 1 details the fluorochromes and fluorescent probes used, and the BD Accuri C6 excitation wavelengths and the detector filter sets used to measure their respective fluorescence spectra.

Retrieval of samples post-analysis required collection of waste fluid from the BD Accuri C6. The C6 system easily permits such collection following optimisation for timing of sample uptake to the point of collection. Spherotech 6-peak and 8-peak validation beads (BD, New Jersey, USA) were used for calibration prior to experimental analysis. BD Accuri raw files were transported to FlowJo 10.8.2 (BD, New Jersey, USA) for quantitative population comparison and data interpretation.

2.3 | MitoTracker green

MitoTracker Green (MTG) (Thermo Scientific Inc; Massachusetts, USA) was diluted to a 100 nM solution in DM. The MTG/DM solution was then added to the wells at 2 mL/well and incubated (37°C/5% CO_2/humidified air) for 30 min. Following incubation, the MTG/DM solution was removed, and fluorescent microscopy was undertaken while cells were still adhered to the plate. Cell monolayers were then washed with sterile PBS and trypsinised and incubated for 5 min (37°C/5% CO_2/humidified air). Thereafter, 800 μL fresh DM was added to neutralize the trypsin and cells were transferred to a 1.5 mL Eppendorf tube before centrifugation at 300 g for 5 min. Cells were then resuspended in sterile PBS. Cellular fluorescence was then measured on the flow cytometer on the FL-1 channel and using fluorescent microscopy with an excitation emission maxima of 490/516 nm.

2.4 | Reactive oxygen species

The ROS sensitive probe CM-H_2DCFDA (Thermo Scientific Inc; Massachusetts, USA) was added to sterile PBS to yield a final concentration of 1 μM. Fluorescent microscopy was undertaken while cells were still adhered to the plate. Cell monolayers were then trypsinised and centrifuged at 300 g for 5 min. The cells were then resuspended in 200 μL CM-H_2DCFDA solution for 15 min (37°C/5% CO_2/

humidified air). Samples were run through the flow cytometer and green fluorescence analyzed on the FL-1 detector (λ_{ex} 488 nm; λ_{em} 533/30).

2.5 | DNA quantification

Live cell DNA quantification was determined using Vybrant DyeCycle Ruby stain (Thermo Scientific Inc; Massachusetts, USA). Cells were trypsinised and centrifuged at 300 g for 5 min, before resuspension in 500 µL of DM. One µl of Vibrant DyeCycle Ruby stain was then added to the cell suspension to yield a concentration of 5 µM. Cells were then incubated for 15 min (37°C/5% CO_2/humidified air) and red fluorescence was then analyzed on the FL-4 detector (λ_{ex} 640 nm; λ_{em} 675/25).

2.6 | Apoptosis

Apoptosis was measured using an Annexin V-FITC detection kit (Thermo Scientific Inc; Massachusetts, USA). Cell monolayers were washed with sterile PBS and trypsinised and incubated for 5 min (37°C/5% CO_2/humidified air) before being centrifuged at 500 g for 5 mins and resuspended in 195 µL binding buffer. Five µl of Annexin V-FITC was then added to the cell suspension, before 10 min incubation at room temperature. Cells were then centrifuged again at 500 g for 5 mins and resuspended in 190 µL of binding buffer. Finally, 10 µL of propidium iodide was added to the cells before subsequent cytometric analysis. Annexin V fluorescence was analyzed on the FL-1 detector (λ_{ex} 488 nm; λ_{em} 533/30), and propidium iodide fluorescence was analyzed on the FL-3 detector (λ_{ex} 488 nm; λ_{em} 670 LP).

2.7 | Myosin heavy chain (MyHC)

Cells were fixed using paraformaldehyde (4%) treatment for 10 min at room temperature. Following fixation of cell monolayers, 500 µL of blocking/permeabilization buffer (0.1% Triton X-100, 0.1% BSA in PBS) was added to the adherent monolayers before incubation for 15 min at room temperature. The permeabilization buffer was removed and cells were then washed twice in sterile PBS. Following washing, a blocking buffer was then added (10% goat serum in sterile PBS) and was incubated for 30 min at room temperature. Cells were then washed further with sterile PBS before the addition of the primary antibody (Myosin heavy chain [MF-20]; Mouse, 1:300, 1% bovine serum albumin [BSA], [DSHB; Iowa, USA] or Glyceraldehyde 3-phosphate dehydrogenase [GAPD]; Mouse, 1:10000, 1% BSA), [Abcam Cambridge, UK]) for an overnight incubation at 5°C. Following overnight refrigeration, the primary antibody was removed, and the cells were further washed in sterile PBS. The secondary antibody (Alexa Flour 488; Goat anti mouse, 1:500) (Thermo Scientific Inc; Massachusetts, USA) was applied and incubated at room temperature for 60 min before further washing in sterile PBS. Fluorescent microscopy was undertaken while cells were still adhered to the plate. Following which, cells were then trypsinised and centrifuged at 300 g for 5 min before resuspension in sterile PBS and analysis by flow cytometry using the FL-1 detector (λ_{ex} 488 nm; λ_{em} 533/30).

2.8 | Fluorescent microscopy

A Leica DMII6000b Microscope (Leica Biosystems; Wetzlar, Germany) was used to capture fluorescently labeled monolayers as it allows for visualization of MitoTracker Green, CM-H_2DCFDA and MF-20 co-visualization with DAPI (Thermo Scientific Inc; Massachusetts, USA). Images of cell monolayers were taken using the 10× objective and 0.5 magnification c-mount fitted to the camera. Blue color channels were used as an indicator of DAPI with the wavelength measured at 358/461 nm (Fluorescent filter; EX: 340–380, DC: 400, EM: 450–490). Green color channels were used as an indicator for MitoTracker Green, CM-H_2DCFDA and MF-20, with the wavelength measured at 499/520 nm (Fluorescent filter; EX: 460–500, DC: 505, EM: 512–542). Image inspection and processing was conducted using Leica Application Suite for Windows 7, (Leica Biosystems; Wetzlar, Germany) and Image J 1.53a (National Institutes of Health; Maryland, USA).

2.9 | Statistical analysis

Changes in flow cytometry fluorescent intensity between myoblasts and myotubes were determined using a two-sample T-test. Myotube sub-population analysis was determined using a one-way between subjects ANOVA. Post-hoc analysis was undertaken using a Tukey's post-hoc test. Data is presented as means ± SD. In all cases an alpha value of <0.05 was considered significant.

3 | RESULTS

3.1 | Optimisation of flow cytometer fluidics settings and sample density

Since changes in fluidics and/or cell sample density can lead to changes in FSC/SSC via the production of cell doublets [21] we determined the optimal fluidic settings, through assessment of several flow rate/core size settings including the standardized slow, medium, and fast settings, alongside additional customized slow-medium and medium-fast fluidics (see Table 2). Our data demonstrated that all fluidic settings fall within the acceptable CV limit of 5% indicating no differences in FSC doublet formation following any fluidic setting. Consequently, all further experiments were performed on the medium fluidic setting. Cells were then analyzed at different seeding densities, all of which fell within acceptable CV ranges (<5%) (see Table 3). However, we did observe an increase in instrumental blockages at higher

TABLE 2 Standard and custom flow rate effects on sample FL-1 fluorescent intensity.

Cells/mL	0.5×10^{-6}		1×10^{-6}		2×10^{-6}	
Flow rate	Slow	Fast	Slow	Fast	Slow	Fast
Average median fluorescent intensity[a]	6146.33	5535.67	6007.67	5376.67	5792.17	5249.67
SD	161.00	194.32	194.90	132.88	19.11	43.56
CV[b]	2.62	3.51	3.24	2.47	0.33	0.83

[a]$n = 4$.
[b]All fluidic settings displayed CV <5%.

TABLE 3 Effect of cell sample density on FL-1 fluorescent intensity under different flow rates.

	Slow	Slow-medium	Medium	Medium-fast	Fast
Flow rate	14 µL/min	25 µL/min	35 µL/min	51 µL/min	66 µL/min
Core size	10 µm	13 µm	16 µm	19 µm	22 µm
Average median fluorescent intensity[a]	5409.38	5680.88	5352.38	5357.75	5287.50
SD	198.53	235.97	191.95	151.30	237.18
CV[b]	3.67	4.15	3.59	2.82	4.49

[a]$n = 3$.
[b]All fluidic settings displayed CV <5%.

sample densities of 1×10^{-6} cells/mL or above, so, 0.5×10^{-6} cells/mL was used for further experiments.

3.2 | Sample gating

Undifferentiated myoblast samples were run on the flow cytometer to determine the myoblast population based on morphology, as reflected in laser scatter properties (See Figure 1A). A distinct, dense population was identifiable as were putatively apoptotic smaller, more granular cells. Counterintuitively, samples of myoblasts that were differentiated to myotubes revealed a residual population of morphologically identifiable myoblasts but, rather than morphologically larger myotubes, a population of smaller cells was manifest and an increase in the number of the putatively apoptotic cell population (Figure 1B).

3.3 | Identification of myotube subpopulations

To enhance distinction of these smaller populations, gating to exclude debris was performed and the selected cells FSC and SSC were plotted on the log scale instead of the standard linear scale to further resolve visual differences. Logarithmic FSC/SSC demonstrated that myoblasts typically gather within a tight group with small amounts of variation between samples. This is expected due to myoblast morphology with very little variation between individual sizes and granularity. However, myotube populations displayed a far greater FSC/SSC variation alongside greater inter-sample variation indicating a larger range in cell morphology. There was, however, a distinct second population identifiable in the myotube samples (see Figure 1C,D).

3.4 | Doublet discrimination

As is routine analysis, doublet discrimination using FSC-H/FSC-A plots was performed. Myoblast populations displayed low doublet detection as opposed to the high doublet detection seen in myotubes (see Figure 1E,F); of course, myotube fusion must be considered when interpreting myotube doublet discrimination. The FSC/SSC plots, however, indicated that the myotubes were of an equal or smaller size to myoblasts causing morphological overlap. Since this is non-intuitive, it suggests that changes in myotube morphology occurred as they were drawn through the cytometer. However, this meant that the robust delineation of myoblast/myotube sub-populations using FSC/SSC alone was impossible using the BD Accuri C6. Due to the heterogeneity of the myotube sample, doublet discrimination resulted in the isolation of individual cell sub-populations, requiring multiple figures to demonstrate both myotube/myoblast populations, which produced the same fluorescent trend (see Figure S1). Therefore, for clarity we opted to measure fluorescent intensity using logarithmic gating. A gating strategy example for a MTG sample is detailed in Figure S2.

3.5 | Metabolic analysis

Due to the unreliable detection of myotubes through morphological analysis, we investigated whether myotube populations would display greater fluorescent intensity using metabolic probes. Given metabolic activity increases following differentiation, any increase in fluorescent intensity would indicate the presence of differentiated myotubes. As expected MTG fluorescent intensity was significantly higher in the myotube population, with an observed 159% increase in fluorescent intensity ($p < 0.0001$) (see Figure 2A–C).

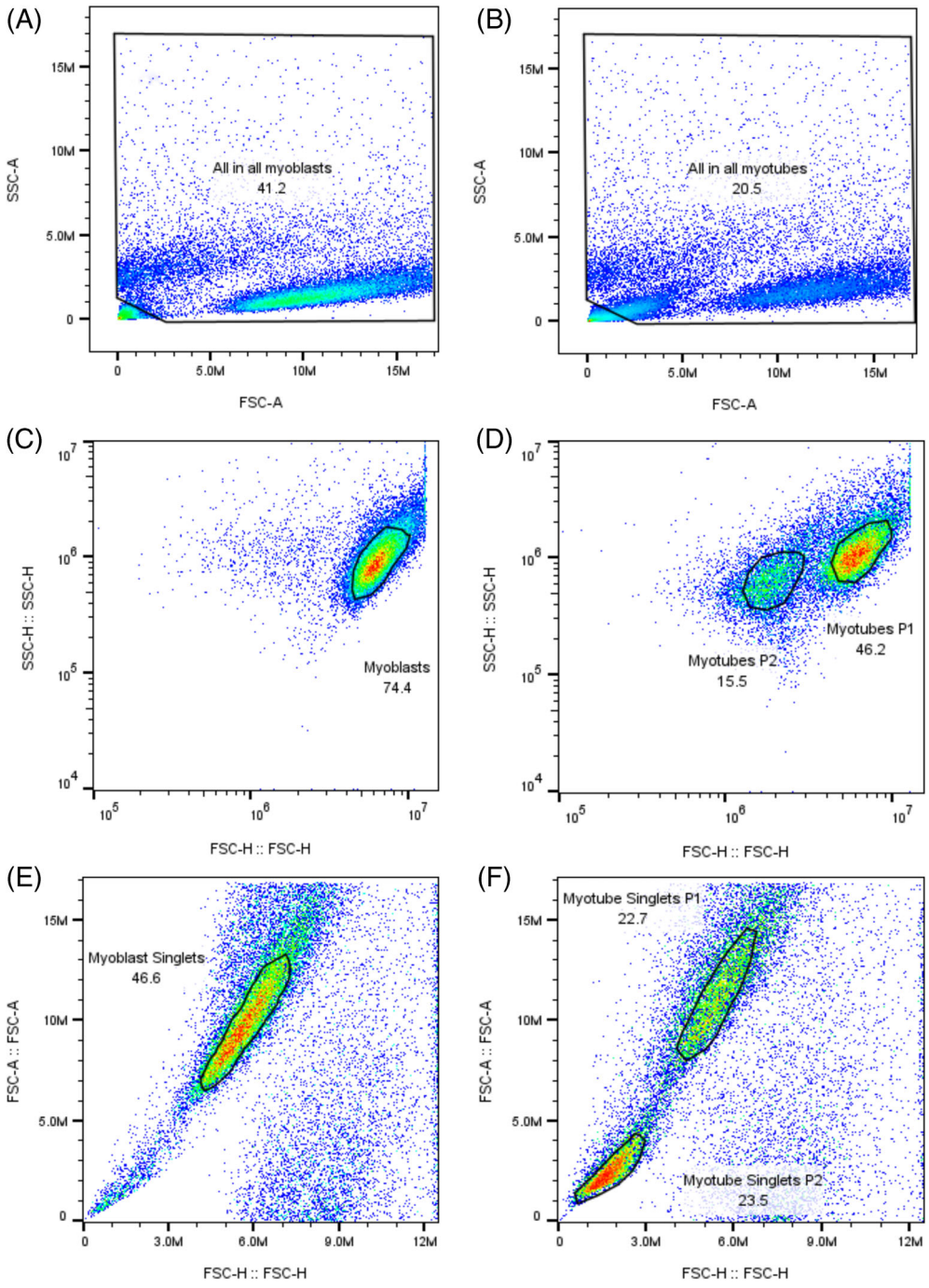

FIGURE 1 FSC/SSC of myoblast (A) and myotube (B) populations. Myotube populations display greater heterogeneity when compared to myoblast. Logarithmic FSC/SSC of both myoblast (C) and myotube (D) populations. (D) demonstrates an overlap of both myotube and myoblast subpopulations within the myotube cell suspension. (E) displays FSC-H/FSC-A doublet analysis indicating a tightly distributed cell population within the myoblast group. (F) Myotube differentiation results in the appearance of a new smaller subpopulation while retaining a significant number of cells in the region of the original myoblast population. [Color figure can be viewed at wileyonlinelibrary.com]

Due to mitochondrial respiration largely contributing to cellular ROS production [22], we then analyzed myoblast and myotube differential staining using the general ROS indicator CM-H_2DCFDA. The CM-H_2DCFDA fluorescent intensity was also significantly higher in myotubes with an observed increase of 303% ($p < 0.0001$) (see Figure 2D–F).

3.6 | DNA quantification

Given that myotubes are multinucleated, it was investigated whether the overall DNA content may differ between myoblasts and myotubes. There was a lack of linear response in the DNA content assessment where one would expect multi-nucleated myotubes to have multiples of the fluorescence of single nucleated blasts and therefore logarithmic analysis was undertaken. The Vybrant DyeCycle fluorescent intensity was 18% higher in the myotube group compared to the myoblast ($p < 0.001$) (see Figure 2G,H).

3.7 | Myosin heavy chain

To confirm the observed changes in metabolic intensity following myotube analysis, we then labeled cells with MF-20 which binds to the motor protein MyHC. Given MyHC is almost entirely expressed in

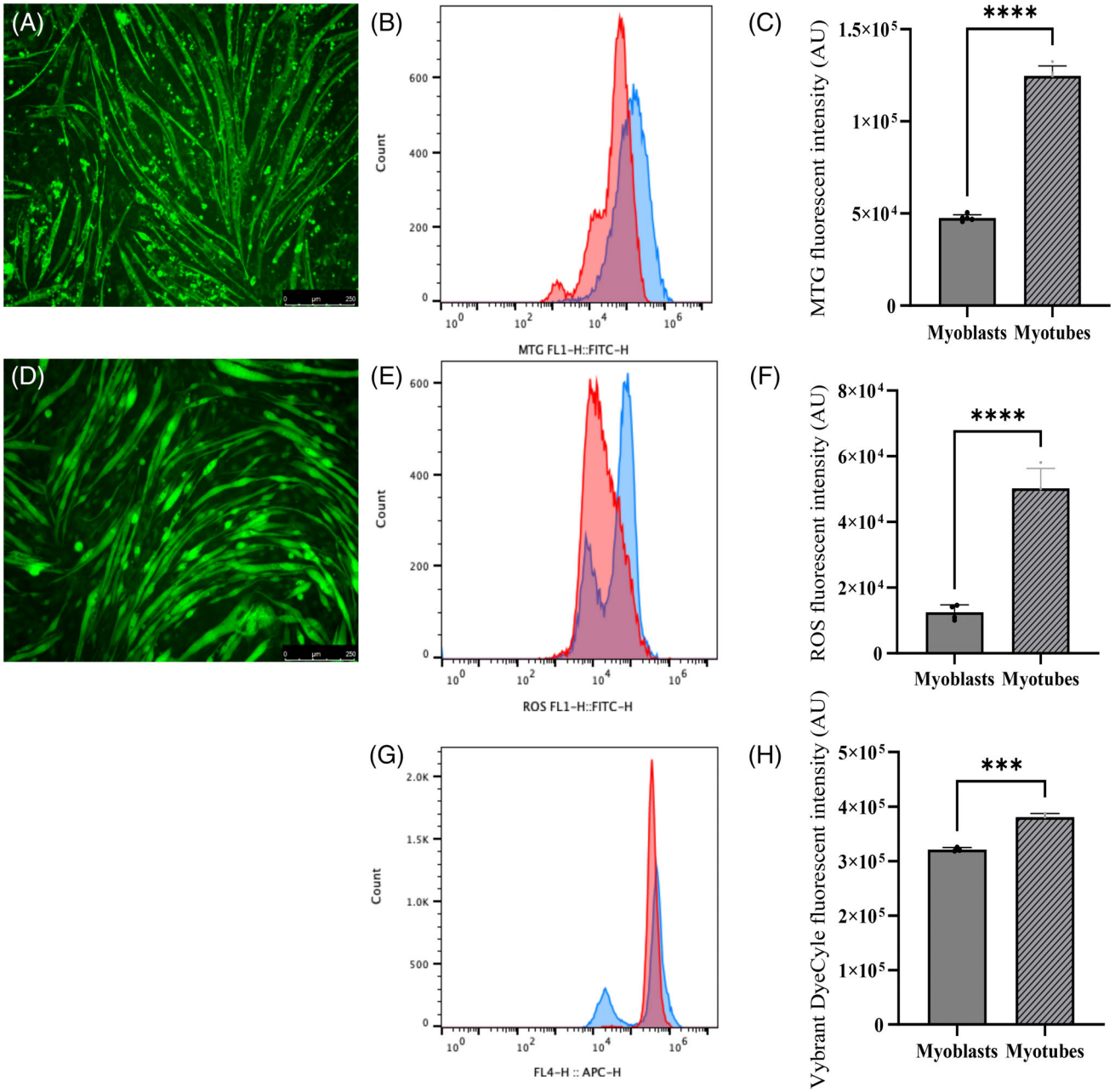

FIGURE 2 (A) Myotube population stained with MTG and imaged prior to cytometric analysis. (B) MTG staining demonstrates a significant increase in FL-1 fluorescence intensity in myotubes (blue) compared to myoblasts (red). (C) This increase corresponded to an 159% increase in median fluorescent intensity reflecting higher mitochondrial mass in differentiated myotubes ($n = 5$, $^{****}p < 0.0001$). (D) ROS (CM-H_2DCFDA) staining of myotube population prior to cytometric analysis. (E) CM-H_2DCFDA staining demonstrates a significant increase in FL-1 fluorescence intensity in the myotube group (blue) compared to the myoblast (red). (F) This increase corresponded to a 303% increase in median fluorescence intensity and reflected increased ROS activity in the myotube population ($n = 4$, $^{****}p < 0.0001$). (G) Cell populations labeled with Vybrant DyeCycle Ruby stain demonstrate a significant increase in FL-4 fluorescence intensity in the myotube group (blue) compared to the myoblasts (red). (H) This increase corresponds to a 18% increase in median fluorescent intensity reflecting a modestly higher increase in DNA content within the differentiated myotubes ($n = 3$, $^{***}p < 0.001$). [Color figure can be viewed at wileyonlinelibrary.com]

myotubes, any changes in fluorescence confirm the presence of differentiated myotubes. Flow cytometry analysis indicated that MyHC fluorescent intensity was 147% higher in myotubes compared to myoblasts signifying the successful analysis of myotube sub populations. Furthermore, we analyzed cells labeled with MF-20 and the nuclear stain DAPI to further demonstrate the fluorescent contrast between the cellular sub-populations ($p < 0.001$) (see Figure 3A–C). Changes in MyHC during cell differentiation are in line with what has been reported previously [14–17], and was also confirmed via western blotting (see Figure S3).

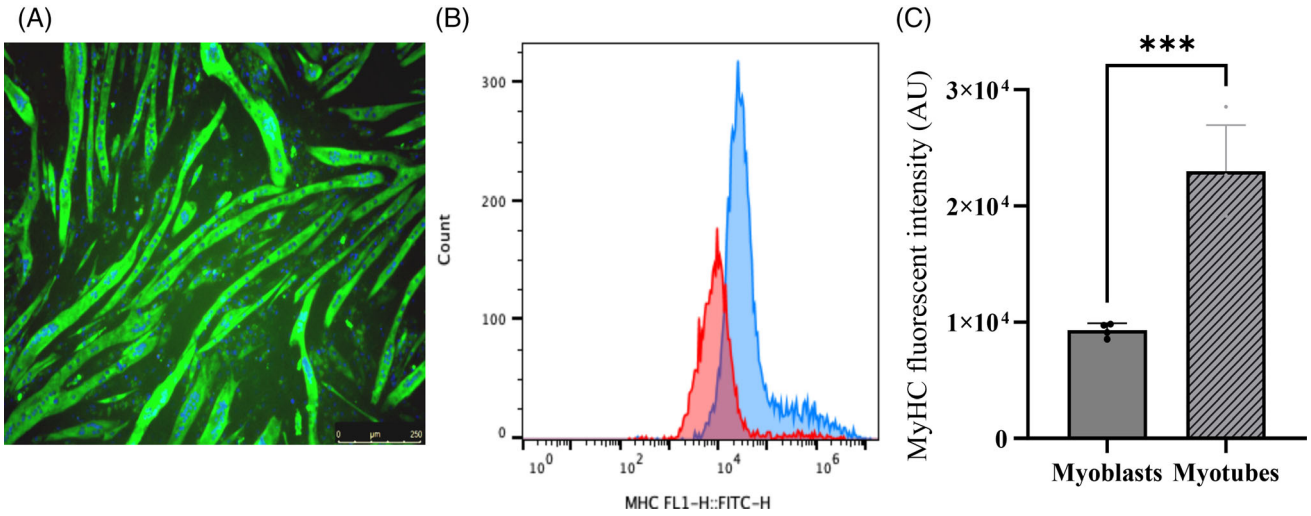

FIGURE 3 (A) Myotubes labeled with the monoclonal antibody MF 20 (green) and the nuclear stain DAPI (blue) to demonstrate the contrast between the cellular sub-populations in terms of myosin Heavy chain (MyHC) expression. (B) MF-20 labelling of MyHC demonstrates a robust increase in FL-1 fluorescence intensity in the myotube group (blue) compared to the myoblast (red) indicating the presence of myosin heavy chain. (C) This increase corresponded to an 147% increase in median fluorescence intensity ($n = 4$, $^{***}p < 0.001$). [Color figure can be viewed at wileyonlinelibrary.com]

3.8 | Sub-population analysis

Having observed an expected increase in both metabolic, nuclear and protein biomarkers following myotube differentiation, we then aimed to determine whether we could characterize the myoblast and myotube sub-populations within a sample to allow for independent analysis of both differentiated and undifferentiated muscle cells concurrently. Myotube P1 population displayed a 180% increase in MTG fluorescence when compared to myoblast controls. Interestingly, the myotube P2 also expressed a significant 55% increase in MTG fluorescent intensity when compared to myoblast controls, indicating that the myotubes fall within both populations ($p < 0.0001$) (see Figure 4A,B).

Changes in cellular ROS content were also measured in the myotube sub-populations where a 464% increase in CM-H_2DCFDA fluorescence intensity was observed in myotube P1 population when compared to myoblast controls ($p < 0.0001$). There was no significant difference between myotube P2 population and control (see Figure 4C,D).

We then attempted to determine whether nuclear content could better resolve the differences between the two myotube sub-populations. The myotube P1 population displayed a 36% higher DNA content fluorescence when compared to myoblast controls ($p < 0.0001$) (see Figure 5A,B). Interestingly, the myotube P2 population demonstrated a markedly lower DNA content fluorescence with an observed 95% reduction when compared to myoblast controls ($p < 0.0001$). Due to the multinucleated nature of myotubes, it was theorized that changes in DNA content may better segregate myotubes from any myoblasts within the P1 population. However, there did not seem to be any clear separation within the P1 population following DNA staining (see Figure 5C).

3.9 | Myotube confirmation

Despite successfully fluorescently labelling myotube sub-populations, it was unclear whether myotubes remain intact and viable during cytometric analysis. Dual labelling with Annexin V and propidium iodide was undertaken to investigate whether myotubes were damaged during the cytometric analysis process. The overall percentage of viable myotubes following Annexin V/Propidium iodide labelling was 81% (see Figure 6A–C). Interestingly, when the myotube sub-populations were analyzed independently, myotube P1 population viability increased to 91% and myotube P2 dropped to 63%. Moreover, there was a significant 28% reduction in viable cells between the myotube P1 and P2 populations (see Figure 6D).

Given that their large size was undetected on FSC, it raised the question whether their morphological characteristics were compromised during analysis. We determined the overall flow time from the point of collection to the waste container using a visible dye and collected the sheath fluid containing the cell suspension. We observed the presence of intact myotubes using brightfield microscopy, demonstrating the successful analysis of myotubes without membrane damage. We also observed the phenomenon of 'rolling up' of myotubes following analysis, which explained the lack of divergence between myoblast and myotube cell sub-populations using FSC/SSC measurements (see Figure 6E,F).

4 | DISCUSSION

We aimed to identify whether differentiated myotubes could be analyzed using flow cytometry and to provide a complete gating strategy for such analysis; something currently absent in the literature. Despite

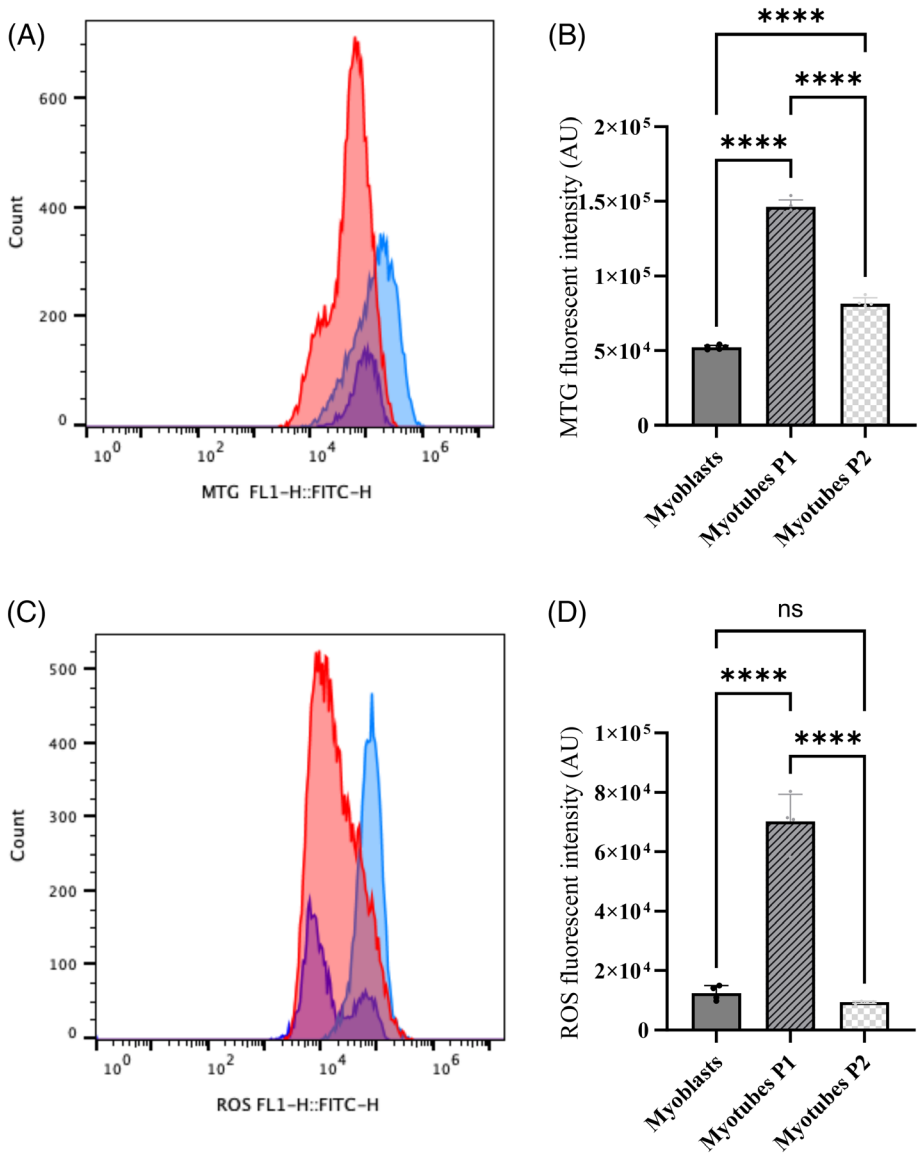

FIGURE 4 (A) MTG staining demonstrates an increase in FL-1 fluorescence in both myotube sub-populations (P1-blue, P2-purple) compared to myoblast (red) sample representing increased mitochondrial mass. (B) This corresponded to a 180% difference in FL-1 fluorescence in population P1 versus control and a 55% increase in population P2 versus control ($n = 5$, $^{****}p < 0.0001$). (C) Comparison of CM-H_2DCFDA staining revealed broad ROS (FL-1 fluorescence) levels in myoblasts (red), which in myotube P1 sub-population (blue) resolved into a uniform population exhibiting an increase in ROS. The P2 (purple) myotube population presented two resolved populations representing both high and low ROS levels. (D) This corresponded to a 464% increase in ROS (FL-1 fluorescence) in population P1 versus control. No significant change observed in P2 ($n = 4$, $^{****}p < 0.0001$). [Color figure can be viewed at wileyonlinelibrary.com]

non-intuitive laser scatter results, which we discuss later, we report that changes in myotube mitochondrial content, ROS production and DNA content can be observed using flow cytometry. Moreover, MyHC expression which is almost entirely expressed following muscle differentiation was markedly higher in the myotube group, thus providing myotube phenotype confirmation. We have demonstrated that myotubes form two distinct morphological (scatter) populations, which differ in viability (annexin V binding). Moreover, we also demonstrate the presence of intact myotubes which present a distinct 'rolled-up' morphological profile during cytometric analysis which we suggest affect the scatter properties as well as some of the fluorescence data obtained. Taken together, all these suggest that differentiated myotubes can be effectively analyzed using flow cytometry with some caveats.

The analysis of myotubes using flow cytometry isn't a new phenomenon [6–9]. However, despite its application, there is little evidence surrounding appropriate gating strategies that meet the International Society for Advancement of Cytometry (ISAC) Minimum Information about a Flow Cytometry Experiment (MIFlowCyt) reporting guidelines to identify myotube sub-populations within the heterogenous cell suspension [23]. To date, there is a lack of definitive evidence documenting the successful analysis of myotubes without membrane damage, calling into question the utility of using flow cytometry for cell viability assays or analyses requiring viable myotubes. Therefore, we outline a gating strategy used for the fluorescent analysis of myotubes which demonstrated an expected increase in cellular metabolic activity and nuclear content, alongside an increase in MyHC expression. Furthermore, we have for the first time proven the presence of viable myotubes following analysis using flow cytometry and outlined the 'rolling' phenomenon that we propose distorts their FSC/SSC, creating non-intuitive scaling of cell populations [24–27].

This non-intuitive scaling of myotube samples may be a key reason for the absence of flow cytometry use with these samples. Herein, we show that myotube sub-populations present less clustered cell populations on a logarithmic scale when compared to myoblasts that is, greater variation in laser scatter parameters reflecting greater

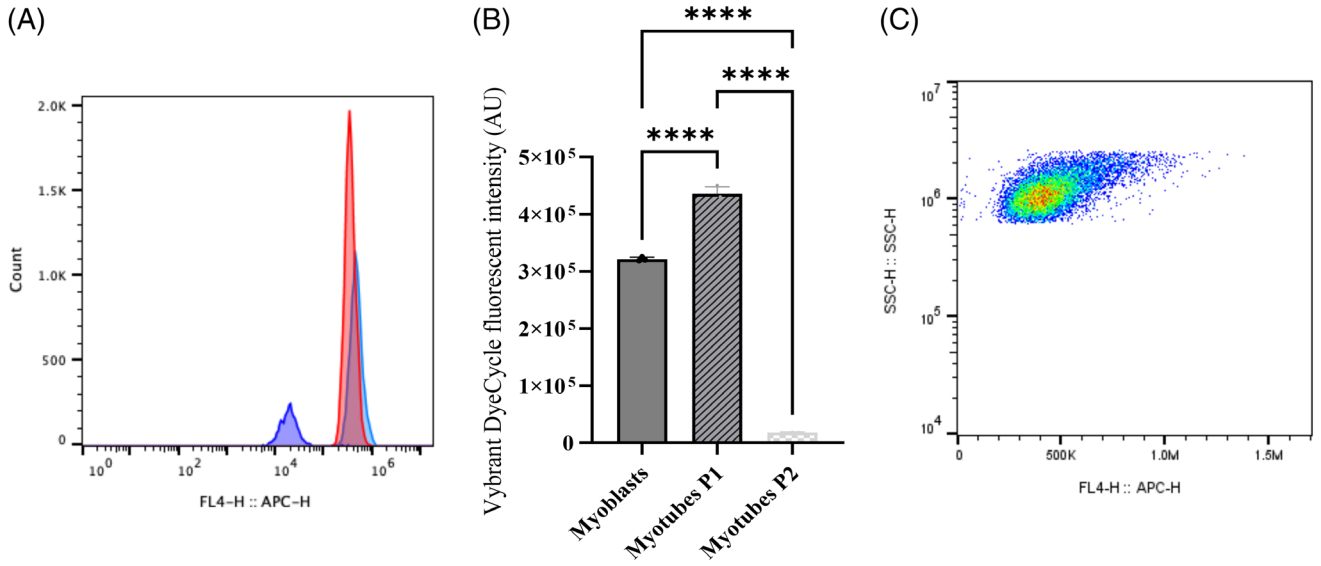

FIGURE 5 (A) Vybrant DyeCycle DNA staining revealed an overlap between the myoblast (red) and myotube P1 (blue) peaks. The myotube P2 population (purple) had a significantly lower fluorescence peak compared to both other populations. (B) This change in DNA fluorescent intensity corresponded to a 36% increase in myotube P1 fluorescence compared to myoblast control. Interestingly, the myotube P2 population demonstrated a 95% reduction in DNA fluorescence intensity compared to the myoblasts. (C) Myoblasts and myotube P1 populations have considerable FSC: SSC overlap however DNA staining was unable to segregate these two populations ($n = 3$, $^{****}p < 0.0001$). [Color figure can be viewed at wileyonlinelibrary.com]

variations in size and granularity. This is perhaps unsurprising given that the size and shape of myotubes can vary substantially compared to single nuclei myoblasts. Indeed, following doublet analysis, the myoblast population presented an anticipated clustering with very few doublets, indicating morphological uniformity of myoblast cell populations. Further to the large differences in the size of the cells being analyzed within myotube samples, we observed myotube samples had a significant number of cells within the same gate originally used to identify myoblasts. Moreover, despite significant morphological overlap between myotube P1 population and myoblast controls, the fluorescent intensity of MTG in P1 was 180% higher than that of myoblasts, indicating metabolic remodeling of the myoblasts. Moreover, sub-population analysis revealed distinct changes in the ROS production within the P2 sub-population, with two distinct peaks observed. The P2 sub-population also demonstrated 95% reduction in DNA content compared to myoblast controls suggesting a lack of cellular events within this population.

Apoptotic bodies are a form of extracellular vesicle produced as a consequence of apoptosis [28]. These vesicles are characterized by the presence of the phospholipid phosphatidylserine (PS) on their outer membrane which is the binding target of Annexin V. Moreover, their larger size in relation to other extracellular vesicles (500 nm-2 μm) means that they are large enough to be detected at the lower end of the FSC:SSC scale [28]. The increase in Annexin V positive staining in the P2 population (31% average) compared to the P1 (6% average), alongside the reduction in DNA content suggests that the P2 population may contain a large population of apoptotic bodies. This observation is not entirely surprising given that myotube differentiation is associated with spontaneous apoptosis [29]. Moreover, myoblast differentiation involves the activation of caspase −9 [30], −2 [31, 32], −3 [32, 33] and is blocked by anti-apoptotic members of the Bcl-2 family [30]. However, this apoptotic phenotype present within a sub-population of differentiating muscle cells has been shown to occur primarily within the myoblasts as myotube differentiation seems to offer apoptotic protection [34]. Therefore, the presence of this P2 population is likely a consequence of the normal myotube differentiation process. Interestingly, apoptotic bodies have been shown to contain intact organelles which may explain why mitochondrial content was higher in the P2 population compared to the myoblast despite a lack of increase observed following ROS or DNA content sub-population analysis. It should also be noted that mitochondrial swelling which would be expected in apoptotic cells and their resultant apoptotic bodies would result in increased fluorescence due to self-quenched probes in the membranes moving apart and increasing their fluorescence yield [35].

Despite evidence suggesting myotube detection via the flow cytometer as measured by increases in metabolic, DNA content and MyHC expression, the FSC: SSC properties did not reflect the larger expected size of the myotubes. Initially, this was assumed to indicate myotube membrane damage/destruction, but viability analysis confirmed an intact, viable sub-population of cells within P1. Therefore, we examined whether myotube morphology was changing through cytometric analysis and if there was, potentially, 'rolling up' contortion of cells through hydrodynamic focussing. We calculated the running time through the BD Accuri C6 and collected samples as they entered the waste container and documented intact myotubes that morphologically resembled myoblasts. This process likely occurred due to the larger size of the myotubes in relation to the core size of

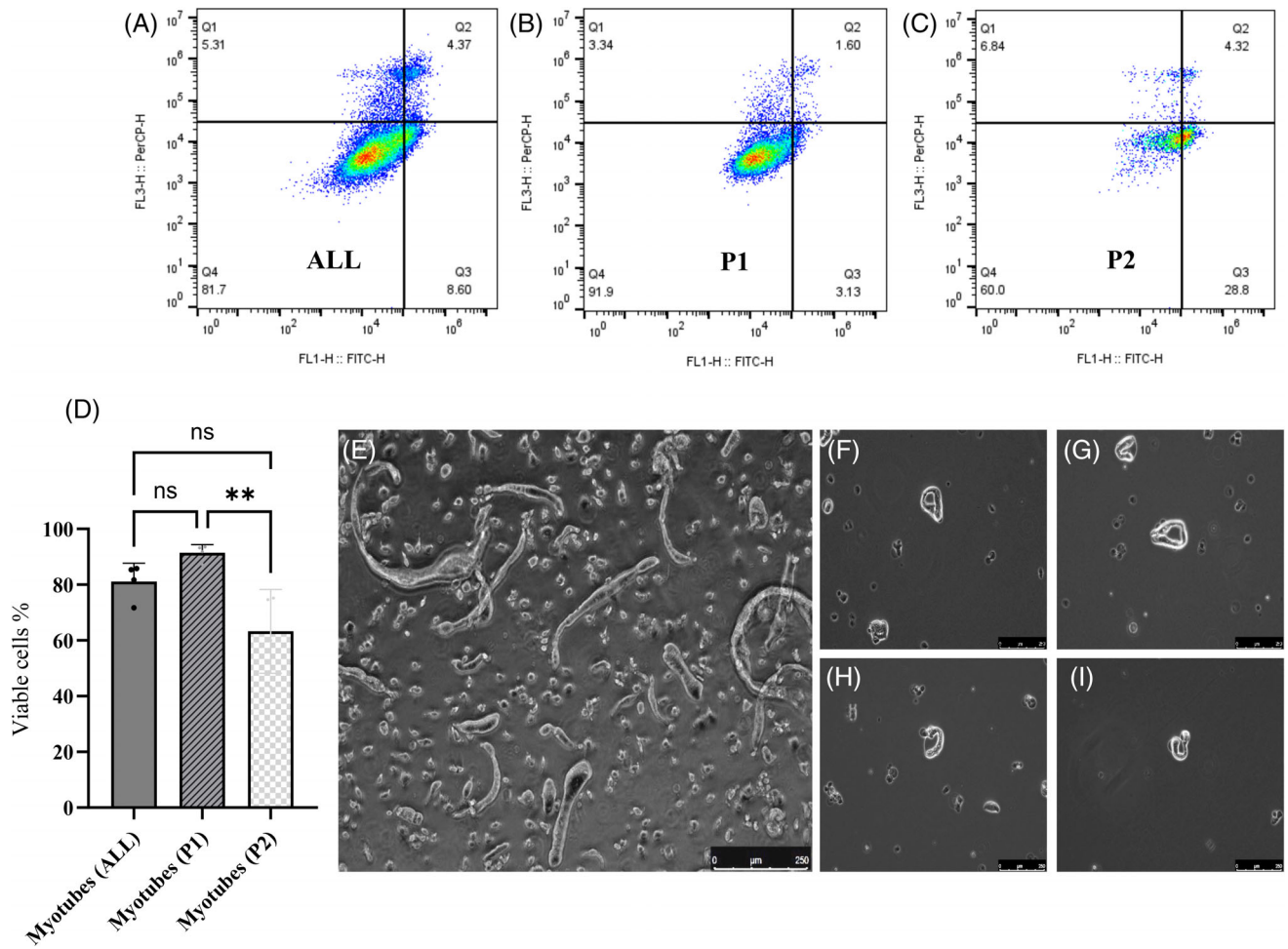

FIGURE 6 (A–C) Annexin V/propidium iodide dual labelling of myotubes prior to analysis via flow cytometry. Overall myotube populations displayed an average of 81% viable cells following analysis. However, further analysis demonstrated that the percentage of viable cells increased further in the P1 sub-population to 91%. Moreover, the P2 sub-population demonstrated a reduction in viable cells with an average of 63% viable cells in quadrant 4. (D) This disparity between the two myotube sub-populations resulted in a 28% reduction in viable cells between P1 and P2. (E) Brightfield microscopy demonstrating myoblast/myotube populations in suspension prior to cytometry analysis. (F–I) Second collection of images demonstrates the presence of intact 'rolled' myotubes following collection at the waste container. [Color figure can be viewed at wileyonlinelibrary.com]

the fluid stream as well as the instruments overall flow cell diameter and resulted in the 'rolling-up' of myotubes to pass through the aperture. Additionally, FSC is a complex measurement of light scattering which can be influenced by a variety of different phenomenon including cell size, refractive index of the nucleus and cytoplasm versus the surrounding medium, absorption properties of the cell, and other factors such as location of the nucleus and other organelles [24–27]. Taken together, this provides an explanation as to why FSC/SSC analysis of myotubes presents a morphological pattern that is not representative of the myotube cell size and shape as seen via microscopy of recovered analyzed cells that were confirmed to be myotubes based on metabolic and MyHC markers of differentiation. Furthermore, it could be possible that the disrupted laser scatter also accounts for a lack of linear response in the DNA content assessment where one would expect multi-nucleated myotubes to have multiples of the fluorescence of single nucleated blasts. We cannot, however, exclude the conjecture that the 'rolled up' morphology (approximately 100 µm in diameter) may extend beyond the laser beams elliptical focus spots (5–20 µm wide and 100 µm high) and into the sheath fluid which would also explain a diminished signal [36]. Acoustic focussing flow cytometry may negate this issue of myotube contortion/'rolling up' and should be further investigated.

The cellular phenotype of myotubes is substantially different to myoblasts. During the process of cellular differentiation, myoblasts undergo metabolic remodeling leading to an increase in mitochondrial capacity and contractile activity [11–13, 18, 19]. As expected, the myotube population presented substantially greater mitochondrial content and ROS production (159% and 303% increase respectively) [18–20]. This is in line with previous findings which have demonstrated a marked increase in mitochondrial respiratory capacity (and subsequent ROS output) following cellular differentiation [18–20]. Indeed, it was interesting to observe that flow cytometry permitted the identification of the two morphological populations in the myotube samples which exhibited unique ROS data suggestive of the

reduced ROS fluorescence within the apoptotic bodies. Ideally, further investigation and multiparameter analysis would help to ratify this and offers an opportunity for future research. In line with the expected metabolic changes, DNA content following myotube differentiation was also 18% higher when compared to myoblasts. It is well reported within the literature that MyHC content is almost entirely expressed in differentiated myotubes and is therefore commonly used as a marker to measure myoblast differentiation [14–17]. Unfortunately, in our current investigation use of MyHC as a definitive marker of myotubes formation was limited in its functionality due to the requirement for fixation of the sample. Consequently, this altered the scatter properties of the observed two populations in unfixed samples. Therefore, assessing the degree to which MyHC was expressed within the two myotube populations was not attainable. However, the 147% increase in MF-20 fluorescence is a clear indication of the expected change in MyHC expression that occurs following myoblast differentiation and the fixed myotubes presented as a uniform population of MyHC positive myotubes. Overall, we concluded that while FSC/SSC analysis remained non-intuitive, fluorescent analysis via flow cytometry provided the expected changes in muscle phenotype that occurs following differentiation and that flow cytometric analysis is a feasible option for myotube analysis.

In summary, our study provides clear evidence highlighting the fluorescence-based detection of myoblast and myotube populations using flow cytometry with insights on the scatter properties that manifest myoblasts and myotubes with similar size properties. This, therefore, provides an evidence base for the use of flow cytometry in multiparameter live cell analysis and immunophenotyping of differentiated muscle populations. We show that differentiated myotube cultures are viable but have discernible and selectable apoptotic body populations which further highlights the import of single cell flow cytometric analysis of myotubes for accurate myotube research. Myotube samples typically present two clear sub-populations and the larger population (P1) shares similar characteristics to myoblasts and contains viable myotubes, with the smaller population (P2) likely containing apoptotic bodies. Moreover, cytometric analysis allows for the specific analysis of viable myotubes within the P1 population which provides an advantage over other alternative methods of analysis. We do, however, caution that given the changes in myotube shape that occur using this method, care should be taken when attempting to infer morphological based data using flow cytometry and that researchers should confirm in their samples that differentiation has occurred; a multiparameter approach easily attained by flow cytometry. Since, we have identified hydrodynamic focussing as the possible cause for myotube cell rolling it would be of benefit to explore the use of acoustic focussing as an alternative system that may provide greater clarity of cell subpopulations and given their resistance to instrumental blockage, may provide a useful alternative than traditional hydrodynamic flow cytometry [37].

FUNDING INFORMATION

Liverpool John Moores University; Rank Prize Fund New Lecturers Award.

PEER REVIEW

The peer review history for this article is available at https://www.webofscience.com/api/gateway/wos/peer-review/10.1002/cyto.a.24822.

ORCID

Andy Nolan https://orcid.org/0000-0001-5514-8414

Darren W. Sexton https://orcid.org/0000-0003-3344-3150

REFERENCES

1. Mauch TJ, Schoenwolf GC. Developmental biology. Am J Med Genet. 2001;99(2):170–1.
2. Chal J, Pourquié O. Making muscle: skeletal myogenesis in vivo and in vitro. Development. 2017;144(12):2104–22.
3. Clemente CF, Corat MA, Saad ST, Franchini KG. Differentiation of C2C12 myoblasts is critically regulated by FAK signaling. Am J Physiol Regul Integr Comp Physiol. 2005;289(3):R862–70.
4. Fortini P, Ferretti C, Iorio E, Cagnin M, Garribba L, Pietraforte D, et al. The fine tuning of metabolism, autophagy and differentiation during in vitro myogenesis. Cell Death Dis. 2016;7(3):e2168.
5. McMahon DK, Anderson PA, Nassar R, Bunting JB, Saba Z, Oakeley AE, et al. C2C12 cells: biophysical, biochemical, and immunocytochemical properties. Am J Phys. 1994;266(6 Pt 1):C1795–802.
6. Munoz J, Zhou Y, Jarrett HW. LG4-5 domains of laminin-211 binds alpha-dystroglycan to allow myotube attachment and prevent anoikis. J Cell Physiol. 2010;222(1):111–9.
7. Turpin SM, Lancaster GI, Darby I, Febbraio MA, Watt MJ. Apoptosis in skeletal muscle myotubes is induced by ceramides and is positively related to insulin resistance. Am J Physiol Endocrinol Metab. 2006;291(6):E1341–50.
8. Muratore M, Srsen V, Waterfall M, Downes A, Pethig R. Biomarker-free dielectrophoretic sorting of differentiating myoblast multipotent progenitor cells and their membrane analysis by Raman spectroscopy. Biomicrofluidics. 2012;6(3):34113.
9. Ebrahimi SM, Bathaie SZ, Faridi N, Taghikhani M, Nakhjavani M, Faghihzadeh S. L-lysine protects C2C12 myotubes and 3T3-L1 adipocytes against high glucose damages and stresses. PLoS One. 2019;14(12):e0225912.
10. Kim M, Sung B, Kang YJ, Kim DH, Lee Y, Hwang SY, et al. The combination of ursolic acid and leucine potentiates the differentiation of C2C12 murine myoblasts through the mTOR signaling pathway. Int J Mol Med. 2015;35(3):755–62.
11. Vivarelli E, Brown WE, Whalen RG, Cossu G. The expression of slow myosin during mammalian somitogenesis and limb bud differentiation. J Cell Biol. 1988;107(6 Pt 1):2191–7.
12. Cho M, Webster SG, Blau HM. Evidence for myoblast-extrinsic regulation of slow myosin heavy chain expression during muscle fiber formation in embryonic development. J Cell Biol. 1993;121(4):795–810.
13. Torgan CE, Daniels MP. Regulation of myosin heavy chain expression during rat skeletal muscle development in vitro. Mol Biol Cell. 2001;12(5):1499–508.
14. Tannu NS, Rao VK, Chaudhary RM, Giorgianni F, Saeed AE, Gao Y, et al. Comparative proteomes of the proliferating C(2)C(12) myoblasts and fully differentiated myotubes reveal the complexity of the skeletal muscle differentiation program. Mol Cell Proteomics. 2004;3(11):1065–82.
15. Sun L, Trausch-Azar JS, Ciechanover A, Schwartz AL. Ubiquitin-proteasome-mediated degradation, intracellular localization, and protein synthesis of MyoD and Id1 during muscle differentiation. J Biol Chem. 2005;280(28):26448–56.
16. Hong J, Park JS, Lee H, Jeong J, Hyeon Yun H, Yun Kim H, et al. Myosin heavy chain is stabilized by BCL-2 interacting cell death suppressor (BIS) in skeletal muscle. Exp Mol Med. 2016;48(4):e225.

17. Zhong X, Wang QQ, Li JW, Zhang YM, An XR, Hou J. Ten-eleven Translocation-2 (Tet2) is involved in myogenic differentiation of skeletal myoblast cells in vitro. Sci Rep. 2017;7:43539.
18. Barbieri E, Battistelli M, Casadei L, Vallorani L, Piccoli G, Guescini M, et al. Morphofunctional and biochemical approaches for studying mitochondrial changes during myoblasts differentiation. J Aging Res. 2011;2011:845379.
19. Sin J, Andres AM, Taylor DJ, Weston T, Hiraumi Y, Stotland A, et al. Mitophagy is required for mitochondrial biogenesis and myogenic differentiation of C2C12 myoblasts. Autophagy. 2016;12(2):369–80.
20. Malinska D, Kudin AP, Bejtka M, Kunz WS. Changes in mitochondrial reactive oxygen species synthesis during differentiation of skeletal muscle cells. Mitochondrion. 2012;12(1):144–8.
21. Cossarizza A, Chang HD, Radbruch A, Akdis M, Andrä I, Annunziato F, et al. Guidelines for the use of flow cytometry and cell sorting in immunological studies. Eur J Immunol. 2017;47(10):1584–797.
22. Balaban RS, Nemoto S, Finkel T. Mitochondria, oxidants, and aging. Cell. 2005;120(4):483–95.
23. Lee JA, Spidlen J, Boyce K, Cai J, Crosbie N, Dalphin M, et al. MIFlowCyt: the minimum information about a flow cytometry experiment. Cytometry A. 2008;73(10):926–30.
24. Meyer RA, Brunsting A. Light scattering from nucleated biological cells. Biophys J. 1975;15(3):191–203.
25. McGann LE, Walterson ML, Hogg LM. Light scattering and cell volumes in osmotically stressed and frozen-thawed cells. Cytometry. 1988;9(1):33–8.
26. Sloot PM, Hoekstra AG, Figdor CG. Osmotic response of lymphocytes measured by means of forward light scattering: theoretical considerations. Cytometry. 1988;9(6):636–41.
27. Scherer JM, Stillwell W, Jenski LJ. Anomalous changes in forward scatter of lymphocytes with loosely packed membranes. Cytometry. 1999;37(3):184–90.
28. Battistelli M, Falcieri E. Apoptotic bodies: particular extracellular vesicles involved in intercellular communication. Biology (Basel). 2020;9(1).
29. Schöneich C, Dremina E, Galeva N, Sharov V. Apoptosis in differentiating C2C12 muscle cells selectively targets Bcl-2-deficient myotubes. Apoptosis. 2014;19(1):42–57.
30. Murray TV, McMahon JM, Howley BA, Stanley A, Ritter T, Mohr A, et al. A non-apoptotic role for caspase-9 in muscle differentiation. J Cell Sci. 2008;121(Pt 22):3786–93.
31. Boonstra K, Bloemberg D, Quadrilatero J. Caspase-2 is required for skeletal muscle differentiation and myogenesis. Biochim Biophys Acta, Mol Cell Res. 2018;1865(1):95–104.
32. Dehkordi MH, Tashakor A, O'Connell E, Fearnhead HO. Apoptosome-dependent myotube formation involves activation of caspase-3 in differentiating myoblasts. Cell Death Dis. 2020;11(5):308.
33. Fernando P, Kelly JF, Balazsi K, Slack RS, Megeney LA. Caspase 3 activity is required for skeletal muscle differentiation. Proc Natl Acad Sci U S A. 2002;99(17):11025–30.
34. Wang J, Walsh K. Resistance to apoptosis conferred by Cdk inhibitors during myocyte differentiation. Science. 1996;273(5273):359–61.
35. Keij JF, Bell-Prince C, Steinkamp JA. Staining of mitochondrial membranes with 10-nonyl acridine orange, MitoFluor green, and MitoTracker green is affected by mitochondrial membrane potential altering drugs. Cytometry. 2000;39(3):203–10.
36. Shapiro HM. Practical flow cytometry. 4th ed. Hoboken, New Jersey, United States: John Wiley & Sons Inc; 2003. p. 736.
37. Li Z, Li P, Xu J, Shao W, Yang C, Cui Y. Hydrodynamic flow cytometer performance enhancement by two-dimensional acoustic focusing. Biomed Microdevices. 2020;22(2):27.

SUPPORTING INFORMATION

Additional supporting information can be found online in the Supporting Information section at the end of this article.

How to cite this article: Nolan A, Heaton RA, Adamova P, Cole P, Turton N, Gillham SH, et al. Fluorescent characterization of differentiated myotubes using flow cytometry. Cytometry. 2023. https://doi.org/10.1002/cyto.a.24822